Cell Communication and Signaling

RESEARCH

Open Access

Sos1 ablation alters focal adhesion dynamics and increases Mmp2/9-dependent gelatinase activity in primary mouse embryonic fibroblasts

Pilar Liceras-Boillos[1†], Rósula Garcia-Navas[1†], Clara Llorente-González[2], L. Francisco Lorenzo-Martin[3], Luis Luna-Ramírez[4], Rocío Fuentes-Mateos[1], Nuria Calzada[1], Francisco M. Vega[5], Mark R. Holt[6], Anne J. Ridley[7], Xose R. Bustelo[8], Miguel Vicente-Manzanares[2], Eugenio Santos[1*] and Fernando C. Baltanás[1,4*]

Abstract

Background Sos1 and Sos2 are guanine-nucleotide exchange factors for Ras and Rac small GTPases, which are involved in a wide range of cellular responses including proliferation and migration. We have previously shown that Sos1 and Sos2 have different effects on cell migration, but the underlying mechanisms are not clear.

Methods Using a 4-hydroxytamoxifen-inducible conditional Sos1^{KO} mutation, here we evaluated the functional specificity or redundancy of Sos1 and Sos2 regarding the control of cell migration and dynamics of focal adhesions (FAs) in primary mouse embryonic fibroblasts (MEFs).

Results Functional analysis of the transcriptome of primary Sos1/2^{WT}, Sos1^{KO}, Sos2^{KO} and Sos1/2^{DKO}-MEFs revealed a specific, dominant role of Sos1 over Sos2 in transcriptional regulation. Sos1^{KO} MEFs had an increased number and stability of focal adhesions (FAs) and curbed protrusion and spreading. Conversely, Sos2^{KO} MEFs displayed unstable FAs with increased protrusion. Interestingly, Sos1, but not Sos2, ablation reduced the levels of GTP-bound Rac at the leading edge. In 3D, however, only Sos1/2^{KO} MEFs showed increased invasion and matrix degradative capacity, which correlated with increased expression of the Mmp2 and Mmp9 gelatinases. Moreover, increased matrix degradation in Sos1/2^{KO} MEFs was abrogated by treatment with Mmp2/9 inhibitors.

Conclusions Our data demonstrate that Sos1 and Sos2 have different functions in FAs distribution and dynamics in 2D whereas in 3D they act together to regulate invasion and unveil a previously undescribed mechanistic connection between Sos1/2 and the regulation of Mmp2/9 expression in primary MEFs.

[†]Pilar Liceras-Boillos and Rósula Garcia-Navas contributed equally to this work.

*Correspondence:
Eugenio Santos
esantos@usal.es
Fernando C. Baltanás
fcalvo@us.es

Full list of author information is available at the end of the article

Keywords Sos1, Sos2, RasGEF, Ras, Rac, Migration, Mmp2/9

Introduction

Ras and Rac proteins are small GTPases that control a wide variety of cellular processes, including cellular proliferation, differentiation, migration and survival. These proteins switch between inactive (GDP-bound) and active (GTP-bound) conformations. GTP binding and its hydrolysis are modulated by negative and positive regulators. GAPs (GTPase-activating proteins) trigger GTP hydrolysis by Ras/Rac, thus inactivating them. Conversely, GEFs (Guanine nucleotide exchange factors) catalyze GTP binding, activating them. Sos (*Son of sevenless*) proteins, Sos1 and Sos2, are the most widely expressed and functionally relevant Ras GEFs [1–5]. In addition to Ras, Sos1/2 activate other related GTPases, including Rac [4–8].

Despite their structural homology, the functional properties of Sos1 and Sos2 are markedly different. Prior analyses of constitutive knockout (KO) strains demonstrated that $Sos1^{-/-}$ mice die during mid-embryonic gestation [6]. Generation of floxed Sos1/2 mice [9, 10] allowed evaluation of the roles of Sos1/2 in different cell lines, tissues and organs under physiological and pathological conditions [8, 11–22]. Most of the studies have been focused on identifying the essential role of Sos proteins, and in particular Sos1, in cellular proliferation [4]. Primary mouse embryonic fibroblasts (MEFs) from $Sos1^{KO}$, $Sos2^{KO}$ and $Sos1/2^{DKO}$ revealed the prevalent role of Sos1 over Sos2 in oxidative, stress-dependent regulation of cell proliferation [12, 18]. These studies laid the foundation for the identification of Sos1 as a potential therapeutic target to treat cancer [4, 11, 14–16, 22–25].

Independent of their role in cell proliferation, Sos1/2 depletion in MEFs impairs cell migration in 2D wound healing assays [18, 26]. Similar observations were made in other lineages such as lymphocytes, macrophages or muscle cells [27–29]. However, more detailed studies are needed to precisely define the specific functional contributions of Sos1/2 proteins in the regulation of cell migration or adhesion.

Here, we use $Sos1^{KO}$, $Sos2^{KO}$ and $Sos1/2^{DKO}$ primary MEFs to demonstrate that Sos1 is a critical mediator of the distribution and dynamics of focal adhesions (FAs) as well as the recruitment of GTP-loaded, activated Rac to the protruding edge of migrating cells. Unexpectedly, Sos1/2 ablation in primary MEFs increased their ability to invade in 3D and degrade gelatin, which is dependent on the increased expression of Mmp2 and 9. Sos1/2 depletion in primary MEFs increased both Mmp2/9 gene and protein expression as well as the Mmp2/9-dependent capacity to degrade gelatin.

Together, these data indicate that Sos1, and Sos2 to a lesser extent, control FA distribution and dynamics and reveal their crucial role in 3D migration through controlling the expression of matrix metalloproteinases.

Materials and methods

Animal models

A mouse strain harboring a floxed version of *Sos1* gene with exon 10 flanked by LoxP sites ($Sos1^{fl/fl}$) [9] was crossed with mice expressing a TAM-inducible Cre recombinase downstream of the RERT (Jackson Laboratories; stock number 017585, expressing an inducible Cre-ERT2, Cre recombinase fused to a triple mutant form of the human estrogen receptor, from the endogenous *Polr2a* locus) promoter to generate homozygous.

$Sos1^{fl.-Cre}/Sos1^{fl.-Cre}$ mice, which were then mated with constitutive $Sos2^{KO}$ mice [30]. Resulting heterozygous mice were subsequently interbred to generate four distinct genotypes used in this report: control ($Sos1/2^{WT}$), Sos1 single-KO ($Sos1^{KO}$), Sos2 single-KO ($Sos2^{KO}$), and $Sos1/2^{DKO}$ [10]. Animals were maintained and euthanized in the NUCLEUS animal facility of the University of Salamanca according to European (2007/526/CE) and Spanish (RD 1201/2005 and Law 32/2007) laws. All experiments were approved by the Bioethics Committee of the Cancer Research Center (#417).

Primary MEF isolation and culture

$Sos1^{WT}$, $Sos1^{KO}$, $Sos2^{KO}$ and $Sos1/2^{DKO}$ primary MEFs were isolated from E13.5 embryos of the corresponding genotypes and used as primary (low passage) cultured cells as previously described [12]. All experimental groups were treated with 4OHT at the indicated time points at each case (H6278, 0.3 µM, Merck Sigma-Aldrich, USA) in DMEM with 10% FBS, glutamine and antibiotics, under identical conditions to induce Sos1 ablation in $Sos1^{KO}$ and $Sos1/2^{DKO}$ experimental groups and to exclude any possible off-target effects in $Sos1/2^{WT}$ and $Sos2^{KO}$ experimental groups. Cells were routinely tested for Mycoplasma (#rep-pt1, PlasmoTest Mycoplasma Detection Kit; InvivoGen).

Incucyte

A total of 1,500 cells per well of DMSO or BI-3406-treated (1 µM) for 24 h were seeded in 96-well culture plates and allowed to grow overnight. Cell growth and morphology were monitored by using the Incucyte® SX5 Live-Cell Analysis System and analyzed with the AI Cell Health Analysis Software Module, which enabled cell identification and area measurement. Readings were taken every 6 h at 20× magnification.

Microarray analysis and RT-qPCR assay

MEFs were treated with 4OHT for 12 days then RNA was isolated from subconfluent MEFs with Nyzol and QIAGEN RNeasy Mini kit (74104, QIAGEN) following the manufacturer's indications. Purified RNA was hybridized to Affymetrix "Clariom S" mouse arrays following the manufacturer's protocol. All data have been uploaded and are accessible at the NCBI Gene Expression Omnibus (GEO) database (GSE277505). R version 3.6.3 was used for statistical analyses along with Python version 3.9 for text file processing. Values of signal intensity were obtained from expression microarray CEL files after robust multichip average (RMA). Differentially expressed genes were identified using linear models for microarray data (Limma). Adjusted P-values for multiple comparisons were calculated applying the Benjamini-Hochberg correction (FDR). Gene Ontology pathway enrichment analyses were performed using DAVID. Expression heatmaps were created using the heatmap3 R package.

mRNA expression levels were determined by quantitative RT-PCR analysis of RNA samples extracted from MEFs. 1 µg of RNA was reverse-transcribed to cDNA (High Capacity cDNA Reverse Transcription Kit; #4368814, Life Technologies). Final concentrations of cDNA were measured (Nanodrop Technologies ND-1000) and adjusted to 0.5 µg/µl. For qRT-PCR analyses, the following gene-specific SYBRGreen-based primers were used: *Mmp2* Fw 5′-caaggatggactcctggcacat-3′ and *Mmp2* Rv 5′-tactcgccatcagcgttcccat-3′, *Mmp9* Fw 5′-gctgactacgataaggacggca-3′ and *Mmp9* Rv 5′-tagtggtgcaggcagagtagga-3′, *β-actin* Fw 5′-cagccttccttcttgggtatg-3′ and Rv 5′-cagccttccttcttgggtatg-3′.

The expression levels of *β-actin* were used as an internal control for normalization. The data were graphically displayed using GraphPad Prism 8. Statistical significance was established at $p < 0.05$.

Immunofluorescence

MEFs were treated for 12 days with 4OHT then fixed with paraformaldehyde (4%) for 10 min and incubated with mouse anti-Paxillin antibody (1:1000, 05-417, clone 5H11; Merck Millipore, Billerica, USA) overnight at 4ºC. Cells were then incubated with Texas Red-conjugated anti-mouse antibody (1:500, Jackson Immuno-Research, West Grove, PA, USA) for 45 min and counterstained with 4,6-diamidino-2-phenylindole (1:1000; DAPI) and Alexa Fluor 488-conjugated phalloidin (1:1000, A12379, Thermo Fisher Scientific (Invitrogen), UK) at room temperature. Images were acquired with a confocal laser-scanning microscope (Leica SP5, Wetzlar, Germany).

To specifically detect Rac activity by immunofluorescence, 4OHT-treated (12d) MEFs were grown on 22 mm type I collagen-coated coverslips (354089 BD Biosciences) to 100% confluency. After 24 h, in vitro scratch assays were performed as described previously [18] with a p10 pipette tip. Cells were fixed 30 min after the scratch in 4% PFA for 15 min at 37ºC. Fixed cells were washed twice with PBS, permeabilized with 0.1% Triton X-100 (Merck Sigma-Aldrich) in PBS for 10 min and incubated with blocking solution containing 5% BSA, 2% goat serum, 0.1% Triton X-100 (in PBS) for 1 h at RT. Coverslips were incubated with 0.3 mg/ml GST-CRIB purified protein (Addgene, Cat#12217) for 1 h at RT, washed three times with PBS and incubated with mouse anti-GST antibody (1:100, sc-138, Santa Cruz Biotechnology) overnight at 4ºC in antibody solution (2% BSA, 2% goat serum and 0.1% Triton in PBS). Coverslips were then washed three times with PBS and incubated with Cy3 anti-mouse antibody (1:500, Jackson ImmunoResearch) and counterstained with DAPI (1:1000) for 1 h at RT in antibody solution. After staining, coverslips were washed three times in PBS and mounted with anti-fading reagent (P36970, Life Technologies). Images were acquired using a Leica DM6000B microscope.

Interference reflection microscopy

Interference reflection microscopy (IRM) uses polarized light to form an image of cells on a glass surface and the intensity of the signal provides a measurement of events happening at the interface of the cell membrane with the substratum, including focal adhesions, which appear as dark patches due to close apposition to the substratum, and other sites of focal contacts including in lamellipodia [31, 32]. MEFs were treated with 4OHT for 9 days and then 1.5×10^5 cells per genotype were seeded on fibronectin-coated (10 µg/ml) 2-cm diameter coverslips. 24 h after plating the cells, using a Zeiss LSM510 confocal microscope, time-lapse sequences of images (every 20 s for 1 h) were taken to generate adhesion maps. The images were processed so that pixels representing FAs stability were colored, red, green or blue corresponding to focal adhesions present early during imaging (red) through to focal adhesions present late during imaging (blue), as previously described [31]. Where contacts were stable, the overlapping frames resulted in a preponderance of white or light grey as a result of merging of the base color. Using ZEN software (Zeiss) the number of lamellipodia and FAs, the area of extension and the stability of FAs were measured and quantified using ImageJ software (NIH v2.0.0).

Using this very same methodology, we were also able to evaluate cell spreading of individual MEFs from the four different genotypes. To do that, we overlapped all images taken for each individual cells (one image every 20 s for 1 h), then generating an image that allowed to examine and measure the spreading of the cell through the time.

Gelatin degradation assay

Gelatin degradation assays were performed as previously described [33]. Briefly, MEFs were treated with 4OHT for 12 days or with the Sos1 inhibitor BI-3406 for 24 h (1μM, HY-125817, MedChemExpress), then 3×10^5 cells per genotype were seeded on coverslips coated with FITC-conjugated gelatin (1 mg/ml; M1303, Biovision, CA, USA) as previously described [33]. After 8 h, cells were fixed in 4% PFA for 15 min and subsequently washed with PBS and incubated in BSA solution (3% in PBS containing 0.1% Triton X-100) for 30 min in the dark at room temperature (RT). The BSA solution was then removed, and samples were stained with Alexa Fluor 568 phalloidin (1:500 in PBS containing 0.3% BSA and 0.1% Triton X-100) for 1 h at RT, protected from light. After washing with PBS, coverslips were mounted with antifading solution medium containing DAPI (1:1000). Images were taken with a laser-scanning confocal microscope (Leica SP5, Wetzlar, Germany). To quantify gelatin degradation, the area fraction (% area that corresponds to degradation) was measured in black and white images using ImageJ (NIH v 2.0.0). Values were normalized to the number of DAPI-stained nuclei.

The effect of the gelatinase inhibitors Ilomastat (S715702, Selleckchem) and ARP-100 (704888-90-4, Santa Cruz Biotechnology, USA) on gelatin degradation was evaluated by plating MEFs on FITC-conjugated gelatin-coated dishes as above. Three hours after plating (to allow the attachment of the cells), Ilomastat (0.5 nM) or ARP-100 (7.5 μM) were added to the medium in serum-free DMEM. After 8 h, MEFs were fixed in 4% PFA and analysed for gelatin degradation as described above.

Wound healing assay

In vitro scratch wound assay was performed as previously described [18] using FIJI software (NIH v2.0.0) to trace movement of individual cells. Briefly, WT primary MEFs were treated with vehicle (DMSO), BI-3406 (1μM), or the Rac inhibitor 1 A-116 (10μM; HY-104064, MedChemExpress) for 24 h, and then the confluent cells of both conditions were scratched with a micropipette tip and closure of the wounded area was recorded for 24 h by using inverted phase-contrast photomicroscopy (Nikon Eclipse Ti-E).

Inverted invasion assay

Inverted invasion assays were performed as previously described [34, 35]. Briefly, 4–5 mg/ml Matrigel (BD Biosciences, #354234) was diluted 1:1 in cold PBS. Then, 100 μl of diluted Matrigel was allowed to polymerize in 8-μm pore transwell inserts (Corning, #353097) for 1 h at 37ºC. Inserts were then inverted, and a total of 6×10^4 primary MEFs (pre-treated with 4OHT for 9 days) of each genotype were seeded onto the outer filter surface and allowed to adhere for 4 h. To remove unattached cells and FBS-containing medium, inserts were washed by dipping in serum-free DMEM and then placed in 500 μl serum-free DMEM containing 0.3 μM of 4OHT as previously described [12]. 100 μl of 10% FBS-supplemented medium were added on top of the solidified Matrigel/PBS mixture to create the chemotactic gradient. Additionally, another set of cells were treated with Ilomastat (0.5 nM) or ARP-100 (7.5 μM). After 72 h, cells were stained with 4 μM Calcein-AM viability marker (C3100MP, Invitrogen) for 1 h at 37ºC. Cells that did not cross the filter were removed with a cotton swabs.

Invading cells were imaged in a Leica SP5 confocal microscope using a 20× objective. Serial optical sections were captured at 2.5u m intervals. The area covered by cells was measured in each section using the Fiji plugin "AreaCalculator" in 8-bit images (threshold 20/255). Relative invasion was calculated as the area covered by cells at each depth of the Z-stack. Two independent experiments in duplicate were performed for each sample.

Western blotting

Subconfluent MEFs that had been treated with 4OHT for 12 days or with BI-3406 (1 μM) for 24 h, were lysed with RIPA buffer. In all cases, 30 μg of total protein were loaded in electrophoresis gels, and immunoblotting was performed as previously described [21]. Primary antibodies used were: rabbit anti-Mmp2 (#4060, 1:1000, Cell Signaling), mouse anti-Sos1 (610096, 1:500, BD, USA), rabbit anti-Sos2 (sc-15358, 1:500, Santa Cruz Biotechnology) mouse anti-phospho-Myosin light chain 2 (#3675, 1:1000, Cell Signaling), rabbit anti-Myosin (#8505, 1:2000, Cell Signaling), rabbit anti-phospho Fak (#sc11765-R, 1:100, Santa Cruz Biotechnology), mouse anti-Fak (#62220, 1:1000, Cell Signaling) and mouse anti-Tubulin (T5293, 1:10000, Sigma). Secondary anti-mouse or anti-rabbit antibodies include goat anti-mouse secondary antibodies (Invitrogen, Cat#A21057; #35521) and goat anti-rabbit secondary antibodies (GE Healthcare, Cat#A21076; #35571).

Statistical analysis

GraphPad Prism (v8.0.1, GraphPad Inc, USA) software was used. One-way ANOVA and Bonferroni's tests were applied for parametrical data, and Kruskal–Wallis and Mann-Whitney U-test for non-parametrical data. For comparisons between vehicle and BI-3406-treated cells, Student's t test was used. Significant differences were considered at p value < 0.05.

Results

Significant transcriptional impact of the ablation of Sos1, but not Sos2, on the transcriptional signature of primary mouse embryo fibroblasts

Our previous studies showed that, in primary MEFs, Sos1/2 are critical mediators of cell proliferation and migration [12, 18]. To investigate how Sos1 and Sos2 might contribute to migration, we initially examined the effect of *Sos1* and *Sos2* genetic ablation (individually or combined) on the transcriptional signature of primary MEFs using microarray hybridization assays (Fig. 1). Multiclass comparisons among the lists of differentially expressed genes obtained under standard cutoff values (FDR = 0.05) revealed dramatic differences in the transcriptomic profile of control Sos1/2^{WT} MEFs from Sos-depleted (Sos1^{KO}, Sos2^{KO} and Sos1/2^{DKO}) MEFs (Fig. 1A). Ablation of *Sos2* alone had the least significant effect on the transcriptional signature of primary MEFs, with only 59 differentially expressed genes relative to their control Sos1/2^{WT} counterparts (Fig. 1A). In contrast, genomic disruption of *Sos1*, alone or in combination with *Sos2*, markedly altered the transcriptional profile of primary MEFs (Fig. 1A), with 2305 differentially expressed genes when *Sos1* was individually ablated and a total of 2506 genes were differentially expressed when both Sos isoforms were deleted (Fig. 1A). Analysis with Venn diagrams revealed that the profile of differentially expressed genes in Sos1/2^{DKO} MEFS involved more significant overlapping with that of Sos1^{KO} than with Sos2^{KO} primary MEFs (Fig. 1B). These results are consistent with a more important role for *Sos1* over *Sos2* in altering transcription in primary MEFs. However, the additive effect observed in Sos1/2^{DKO} cells compared to Sos1^{KO} cells suggested the possibility of a potential, partial functional redundancy of Sos2 that only becomes detectable when Sos1 is absent.

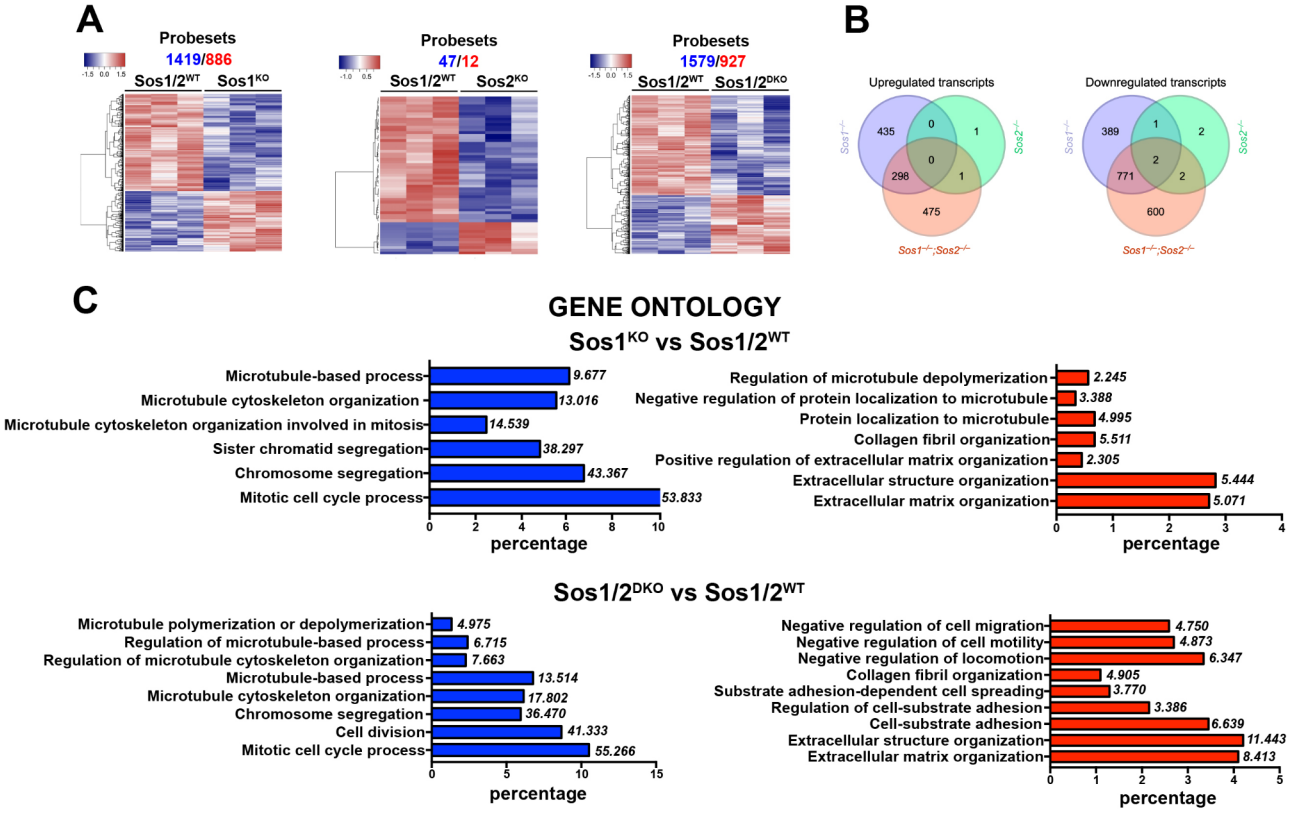

Fig. 1 Sos1, but not Sos2, depletion significantly affects the transcriptional signature of primary MEFs. (**A**) Pairwise comparisons of differential gene expression among different Sos1/2 genotypes. A set of 12 independent chip microarray hybridizations ($n = 3$ independent sample per genotype) were performed using RNA extracted from actively growing primary MEFs belonging to the indicated genotypes. The heatmaps show the results of hierarchical clustering and multiclass comparisons identifying the upregulated (red) and downregulated (blue) probesets that showed significant differential expression at stringent conditions (FDR = 0.05) when comparing Sos1/2^{WT} primary MEFs with the rest of experimental groups. Total number of repressed (blue) and upregulated (red) differentially expressed probesets detected in these comparisons is indicated on top of each heatmap. Values in each horizontal chart indicate -Log P. (**B**) Venn diagrams display the relations between the lists of differentially expressed genes (DEGs) in the three sets of comparisons. (**C**) Functional annotation of DEGs. Text on the left side of the graphs identify functional categories that are enriched at elevated statistical significance within the lists of DEGs (red: overexpressed; blue: repressed) included in the clusters identified in Sos1/2^{WT}-Sos1^{KO} and Sos1/2^{WT}-Sos1/2^{DKO} pairwise comparisons. The bars represent the percentage of the total number of differentially expressed repressed (blue) or overexpressed (red) gene probe sets ascribed to specific groups of genes of each of the above dendrograms that were identified as significantly enriched (hypergeometric p-values in italics)

Functional annotation analysis of the differentially expressed genes in the dendrograms showed that the subset of repressed genes in Sos1^{KO} primary MEFs, which include both Sos1^{KO} and Sos1/2^{DKO} cells, is significantly enriched in functional GO categories generally linked with cell cycle and cell division together with microtubule cytoskeleton organization (Fig. 1C). On the other hand, clusters containing upregulated genes in Sos1^{KO} MEFs included genes linked to extracellular matrix organization and regulation of cell adhesion, as well as negative regulation of cell migration (Fig. 1C). In contrast, differentially expressed genes in Sos2^{KO} MEFs did not display functional clustering.

Overall, our data reveal that *Sos1* ablation induces much more significant alterations of the MEF transcriptional profile than *Sos2*, and that a major subset of genes altered by the absence of Sos1 include regulators of the cellular cytoskeleton and cell migration.

Sos1/2 depletion affects cellular morphology and focal adhesion distribution and dynamics

We have reported previously that Sos1 lack of expression, individually or combined with Sos2, altered the actin cytoskeleton and impaired MEF proliferation [12, 18]. Consistently, transcriptomics analysis of Sos1^{KO} MEFs revealed an upregulation of genes involved in the repression of cell migration, correlating with a significant reduction of the ability of these cells to migrate in in vitro and in vivo wound-healing assays [18, 19].

Cell migration is coordinated by dynamic changes to the actin cytoskeleton and integrin-mediated FAs [36, 37]. To understand how Sos1/Sos2 protein depletion reduces cell migration, we analyzed the effects of Sos1 and Sos2 ablation on the distribution and dynamics of FAs and the actin cytoskeleton (Fig. 2). Sos1^{KO} and Sos1/2^{DKO} MEFs displayed an aberrant distribution of actin cables, which were shorter and more radial, with frequent retraction edges that resulted in apparently smaller, isometric, and flattened cells. These actin fibers were capped by short FAs throughout the periphery of the cell as well as more central positions, revealed by staining with an anti-paxillin antibody. By contrast, Sos1/2^{WT} and Sos2^{KO} MEFs displayed a regular elongated fibroblastic morphology including an abundance of shape-defining stress fibers ending in long FAs (Fig. 2). In these cells, FAs were mainly restricted to the two main poles of the cells (Fig. 2, white arrows).

We used interference reflection microscopy (IRM) to analyse dynamic changes in sites of closest contact with the substratum, which represent FAs as well as smaller adhesive sites in lamellipodia [31]. FAs in both WT and Sos2^{KO} MEFs were mainly restricted to the poles of elongated cells, showing less strong signal in comparison with Sos1-devoid MEFs and displaying morphologies mainly parallel to the longitudinal axis (Fig. 3A, B). In contrast, FAs in Sos1^{KO} MEFs (Sos1^{KO} and Sos1/2^{DKO}) were observed around the whole circular cell perimeter and with a random organization (Fig. 3A, B). Quantitative measurements revealed that the number of FAs per cell was significantly higher in Sos1^{KO} MEFs than in Sos1/2^{WT} and Sos2^{KO} MEFs (Fig. 3F). Interestingly, Sos2^{KO} MEFs displayed a modest reduction in the number of FAs compared to control MEFs (Fig. 3F). These data suggested that Sos1 deletion impaired adhesion maturation. To address this, we generated pseudo-colored IRM images representing the position of the cell contacts at the beginning of the analysis (in red), at half time (in green) and at the end (in blue) of the recording. White color indicates a superposition of red/green/blue colors and represents a static FA (Fig. 3E). We observed that both Sos1/2^{WT} and Sos2^{KO} MEFs displayed more dynamic cell contacts consistent with a polarized migratory behavior, whereas Sos1^{KO} MEFs exhibited a more static condition, with non-polarized motility of the cell membrane (Fig. 3E). Moreover, Sos1/2^{DKO} MEFs barely modified their contact positions (Fig. 3E, note the mostly white display), indicating that concomitant Sos1/2 depletion severely affected the dynamics of FAs and the migratory ability in MEFs. We next hypothesized that impaired adhesion maturation would impair cell spreading. Cell area analysis revealed that Sos1^{KO} cells were slightly smaller than control and Sos2^{KO} cells (Fig. 3H), indicating a deficient ability to spread. Consistently, dynamic analysis of the number of extended lamellipodia, indicative of protrusive migration, per cell revealed that Sos1^{KO} cells displayed a significantly lower number of protrusions than control or Sos2^{KO} cells, which in turn had a slightly higher number of protrusions than control cells (Fig. 3I).

Taken together, our observations indicate that Sos1 depletion in MEFs, alone or in combination with Sos2 deletion, results in an increase in the number of FAs and fewer lamellipodia per cell that correlate with a high proportion of stable FAs and a reduction in the cell spread area, impairing cell spreading and hence the ability of the cell to migrate. Our data also indicate a specific role for Sos2 in membrane protrusion and cell adhesion that is superseded when both isoforms are deleted simultaneously.

Sos1 ablation specifically alters the localization of activated Rac in F-actin rich domains and decreases cellular contractility

In addition to Ras, Sos1 activates Rac [7, 8, 38]. While the exact mechanism of Rac activation by Sos1 is still poorly understood, some data point to the crucial role of Sos1 in the control of lamellipodial protrusion, cell migration and invasion [4, 7]. Using Sos^{KO} MEFs we

have previously shown that the global levels of cellular GTP-bound Rac (in pull-down assays) remained unaltered upon individual or combined Sos1/2 depletion when compared with WT control cells [18]. However, Sos1 could control the spatial dynamics of Rac activation while having no effect on the global levels of activated Rac. To address this possibility, we localized active Rac-GTP by immunofluorescence in Sos1/2^{KO} MEFs upon wound healing (Fig. 4). These experiments revealed that Rac-GTP clusters at the free edges of Sos1/2^{WT} and Sos2^{KO} MEFs (Fig. 4). Conversely, Sos1^{KO} and Sos1/2^{DKO} MEFs did not display Rac-GTP clustering at free edges, being only detectable in the cytoplasm of cells (Fig. 4).

Since protrusion and retraction are tightly coordinated to mediate cell migration [37], we also examined the contractile status of the cell using phosphorylation of the regulatory light chain of myosin II as a fiduciary marker of contraction [39]. We observed a marked reduction in the levels of phospho-myosin light chain 2 (Ser19) in Sos1^{KO} MEFs (Sos1^{KO} and Sos1/2^{DKO}) compared to Sos1/2^{WT} and Sos2^{KO} MEFs (Fig. 5). These data correlate well with the observed morphological effects of Sos1^{KO} MEFs (Figs. 1 and 2) and with the reported effect of the reduction of the levels of RLC or its activation in mesenchymal cells [40]. Overall, these results suggest that Sos1 is required for the local activation of Rac at prospective protruding edges of migrating cells. Given that, this effect is likely confined to migrating cells, which comprise a small percentage of the total cells in a wound healing assay, these results are compatible with the lack of effect of Sos1 depletion in the global levels of Rac activation, as reported previously [10].

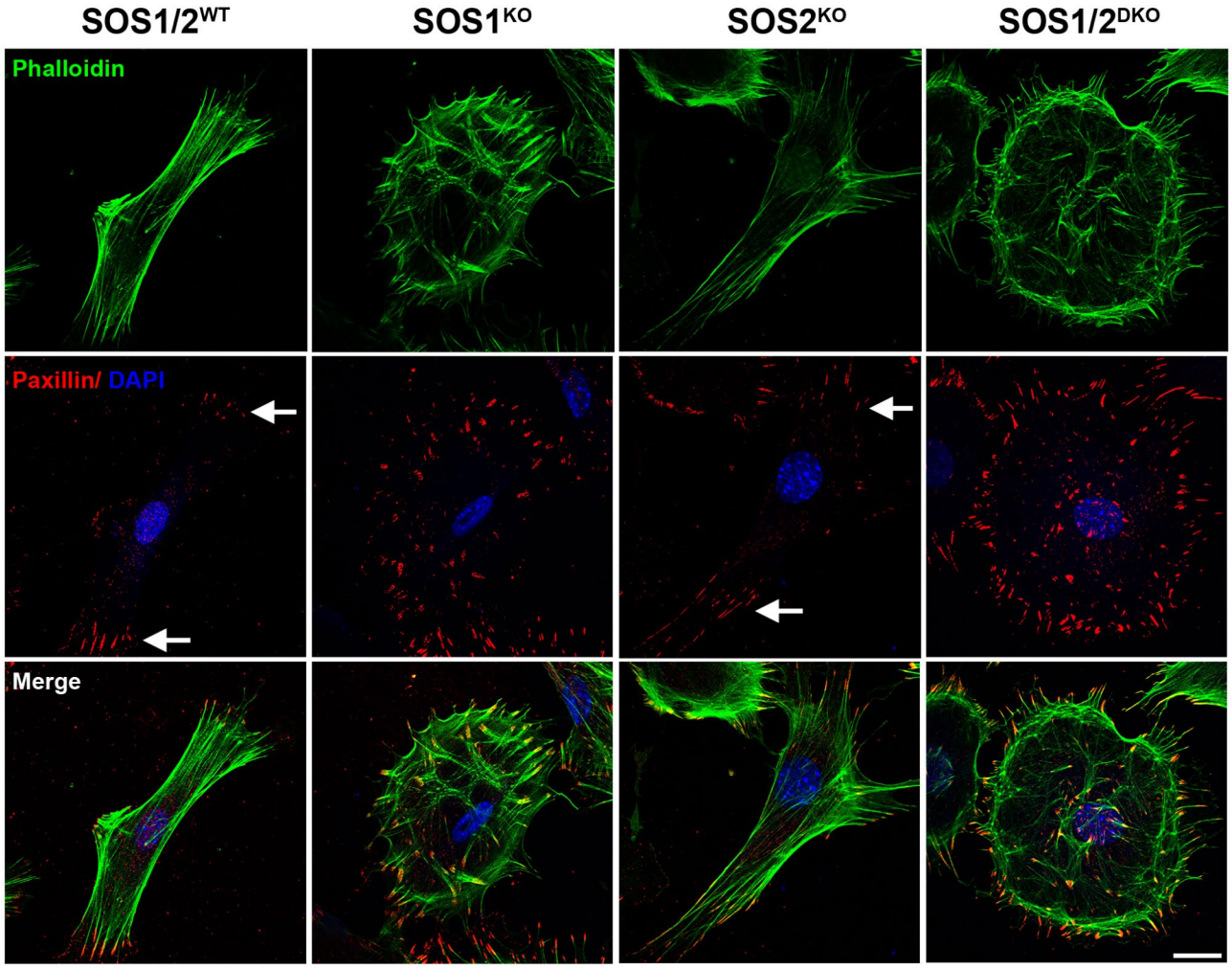

Fig. 2 Sos1 depletion alters focal adhesion and F-actin distribution in primary MEFs. Representative confocal microscopy images of individual primary MEFs from the four genotypes (Sos1/2^{WT}, Sos1^{KO}, Sos2^{KO} and Sos1/2^{DKO}) stained with for actin filaments with phalloidin (green), focal adhesions (FA) with anti-Paxillin antibody (red) and for nuclei with DAPI (blue). Arrows show predominant areas of FA localization in Sos1/2^{WT} and Sos2^{KO} MEFs. Scale bar: 25 µm

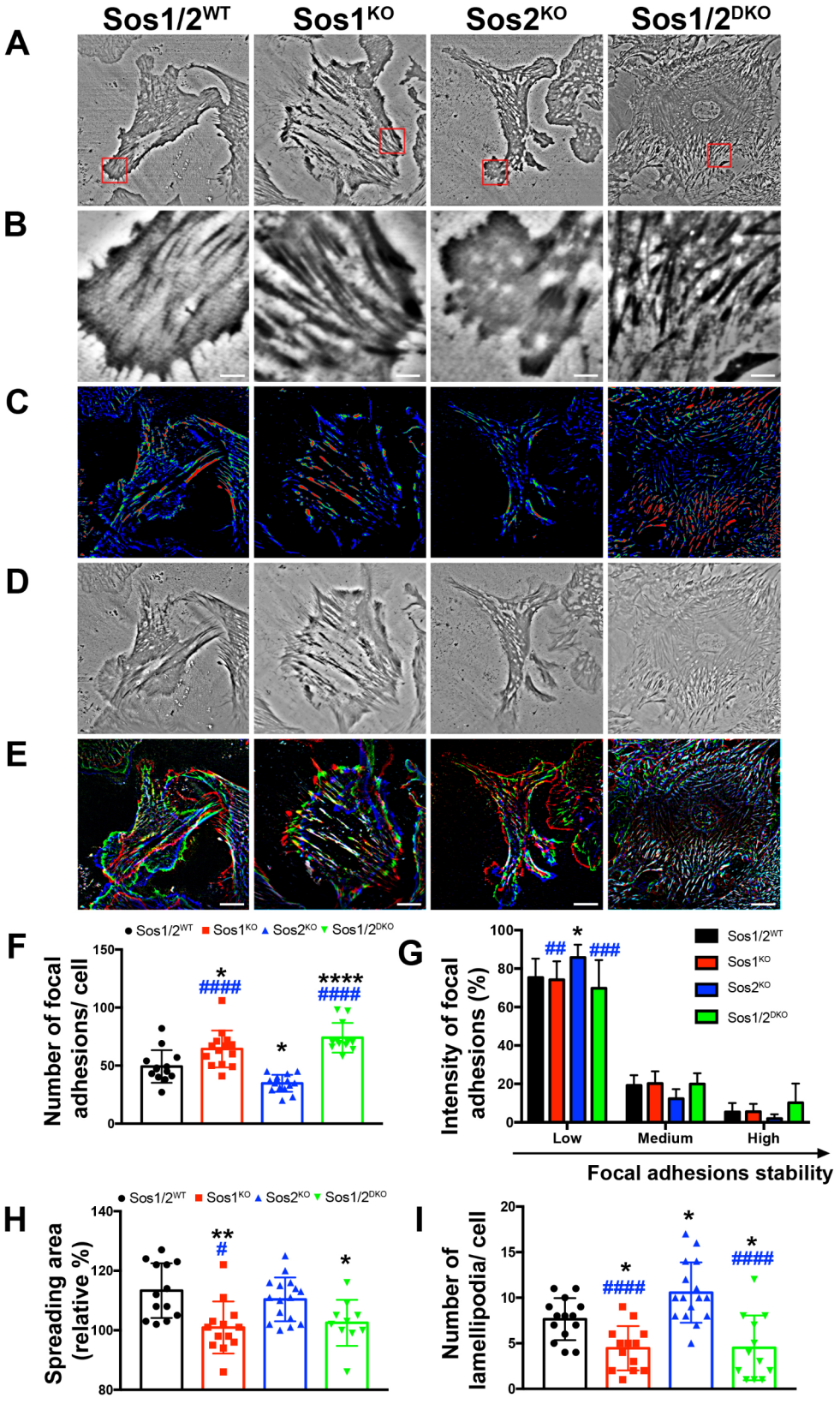

Fig. 3 (See legend on next page.)

(See figure on previous page.)

Fig. 3 Sos1 depletion alters focal adhesion dynamics. **(A)** Representative IRM images of individual primary MEFs from the four indicated genotypes, taken from timelapse microscopy movies. Boxes indicate regions shown in enlarged images in **(B)**. Scale bar in B: 10 µm. **(C)** Individual MEFs in A are represented with a color code (red, green and blue) representing the stability of FA throughout the duration of the timelapse experiments (60 min) scaling from low (blue), medium (green) and high (red) stability, respectively. **(D)** Cell spread area of MEFs from the four genotypes was evaluated by IRM. Images were generated by serially overlapping all movie images (1 image every 20 s during 60 min). **(E)** Images illustrate the cell perimeter of individual MEFs at different time points using a color code that represents the relative cell position at the beginning of the experiment (time 0, red) at 30 min (green) and at 60 min (blue), respectively. In addition, white color represents convergence zones and illustrates highly stable FA. Scale bar: 25 µm. (**F**-**I**) Bar charts represent the number of FA per cell (**F**) the relative percentage of intensity of FA (**G**), cell spread area (**H**) and the number of lamellipodia per cell in MEFs of the four genotypes. $n = 12$ cells per genotype (from three experimental replicates) (**F** and **I**), $n = 9$ per genotype (from three experimental replicates) (**G**) and $n = 10$ per genotype (from three experimental replicates) (**H**). Data are expressed as mean ± SEM. Statistical differences were considered at: */# $p < 0.05$, **/## $p < 0.01$ and ***/### $p < 0.001$ vs. Sos1/2^{WT} and Sos2^{KO}, respectively

Sos1/2 depletion facilitates invasive migration of MEFs in 3D culture

In 2D, Sos1 is crucial for cell migration in a Rac-dependent manner [18]. In this regard, our results demonstrated that Rac inhibition resulted in similar impairment in wound closure as detected with the Sos1 inhibitor, BI-3406 (Supplementary Fig. 1). However, multiple studies have highlighted the large differences in signaling, adhesion, traction and matrix reorganization in cells migrating in 3D (reviewed in [41]). To study the behavior of Sos^{KO} MEFs in 3D migration, we performed inverted Matrigel invasion assays [35]. Surprisingly, both Sos1 or Sos2 ablation, individually or combined, significantly increased the invasion of a 3D Matrigel matrix when compared to their Sos1/2^{WT} counterparts (Fig. 6). In addition, Sos2^{KO} cells tended to invade less than Sos1 lacking MEFs (Fig. 6).

While 2D migration depends almost exclusively on cycles of membrane protrusion and cell body retraction [42], 3D migration of mesenchymal cells also requires matrix reorganization and degradation [43]. The opposite effect of Sos1 depletion in 3D migration compared to its effect in 2D suggested that its role in protrusion/retraction could be superseded by another type of defect. To address this, we measured the levels of Mmp2/9 (*Mmp2* and *Mmp9* genes), which are canonical matrix metalloproteases involved in the degradation of collagens and some other matrix proteins during 3D migration, including collagen IV, which is present in Matrigel [44–46]. These experiments revealed that *Mmp2* mRNA was significantly overexpressed in Sos1/2^{DKO} cells when compared to the rest of experimental groups (Fig. 6A). Conversely, individual Sos1 or Sos2 depletion had a much lower, but still significant, effect on *Mmp2* expression (Fig. 6A). Western blot experiments also revealed increased expression of Mmp2 protein (Fig. 6B). On the other hand, individual ablation of Sos1 and Sos2 increased expression of *Mmp9*, but the simultaneous depletion of Sos1 and Sos2 had almost no effect compared to WT MEFs (Fig. 6A). These data suggest that Sos1 and Sos2 normally suppress *Mmp2* and *Mmp9* transcription, and thus depletion of either Sos1 or Sos2 increases *Mmp2* and *Mmp9* levels.

Sos1/2 ablation increases gelatin degradation activity in MEFs

To test whether Sos1/2 depletion increased the ability of MEFs to degrade extracellular matrix in a Mmp2/9-dependent manner, we studied the effect of Sos1/2 depletion in a 2D gelatin degradation assay (Fig. 7). We found that single or combined Sos1/2 depletion significantly increased the ability of MEFs to degrade gelatin as compared to WT MEFs (Fig. 7A). Interestingly, Sos1^{KO} MEFs exhibited a slightly higher ability to degrade gelatin than their Sos2^{KO} counterparts (Fig. 7A).

We tested whether gelatin degradation was dependent on Mmp2/9 by treating the cells with selective inhibitors for these Mmps (ARP-100 and Ilomastat, Fig. 7B and C, respectively). We found that these Mmp inhibitors blocked Sos1/2-dependent gelatin degradation almost completely, independent of their genotype (Fig. 7B, C). These experiments support a model in which the enhanced gelatin degradation observed in Sos1/2-depleted cells depends on their increased expression of Mmp2/9.

Pharmacologic Sos1 inhibition does not recapitulate in vitro genetically-mediated Sos1 ablation in primary MEFs

During recent years, pharmacological inhibitors with demonstrated ability to directly block Sos1::RAS interactions have been developed [4]. In this regard, BI-3406 has been proven as a potent, selective and orally available, Sos1 inhibitor [24]. We then aimed at evaluating the effect of BI-3406 administration in WT primary MEFs.

We first examined whether pharmacologic inhibition of Sos1 caused morphological alterations in the cell cytoarchitecture of primary MEFs. Our results showed that BI-3406 administration in, WT MEFs, barely modified cell morphology, only exhibiting a slight increase in cell area, without a loss of the polarity, or did not affect to the protein expression levels of phospho-Myosin in comparison with the vehicle-treated counterparts (Fig. 8A, D, E). Cell count measurement in cultures of BI-3406-treated primary MEFs of the WT genotype revealed that, pharmacologically-mediated Sos1 inhibition did not impact the cell growth of primary MEFs (Fig. 8B). We next examined the effect of BI-3406 in the regulation of cell

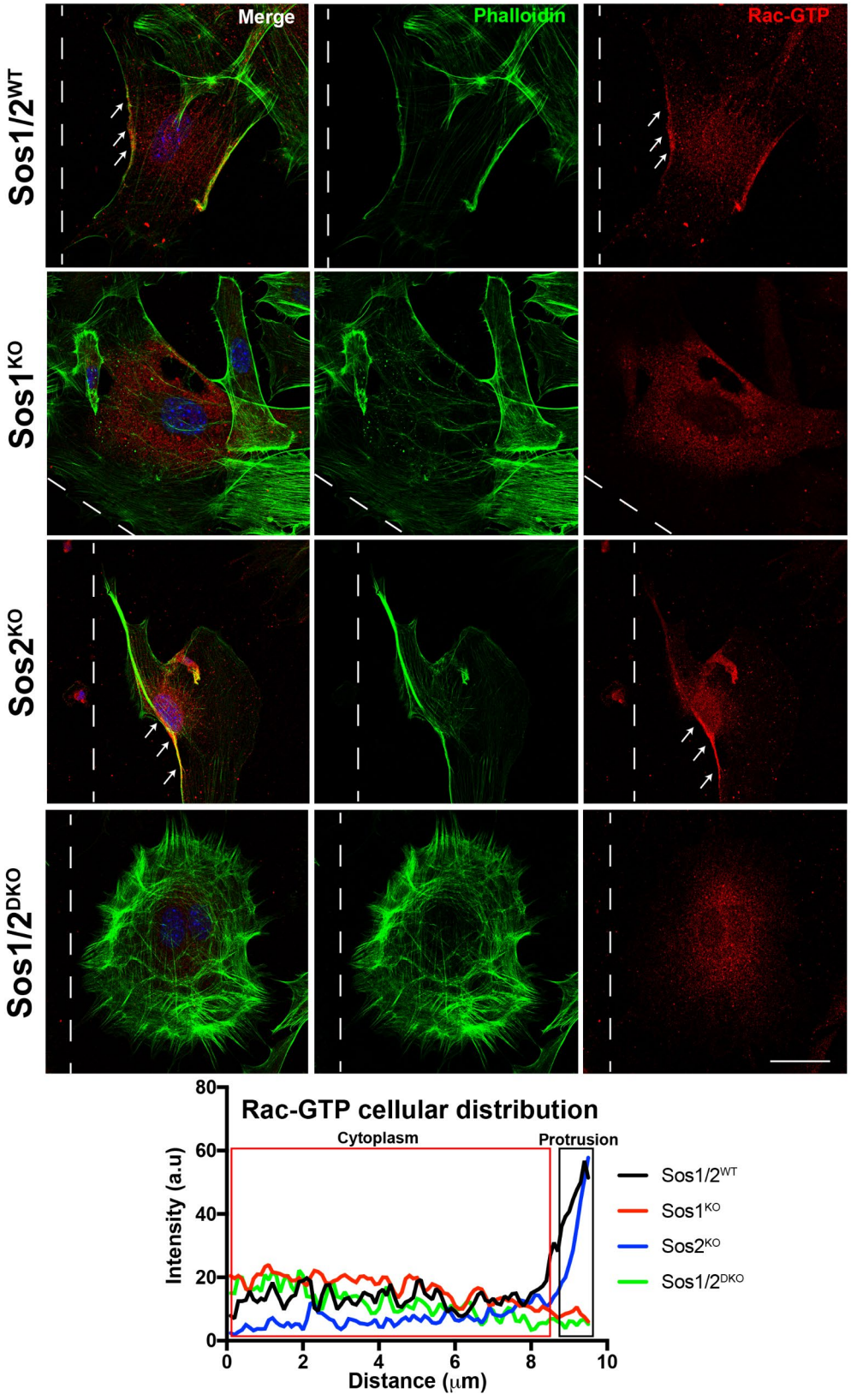

Fig. 4 (See legend on next page.)

(See figure on previous page.)

Fig. 4 Sos1 depletion alters cellular Rac-GTP localization. Representative confocal microscopy images of primary MEFs of the four defined experimental groups stained with for actin filaments with phalloidin (green), with GST-PBD followed by anti-GST antibodies to detect GTP-loaded Rac (red) and with DAPI to stain nuclei. Dotted lines indicate the site of the scratch. Arrows indicate accumulation of Rac-GTP near to the scratched sites at 30 min after the scratch. Scale bar: 10 µm. The plot shows the mean intensity of Rac-GTP immunoflorescent signal in MEFs of the four defined groups, through the cytoplasm and the free edges, of all experimental groups. The intensity was quantified by measuring the signal intensity using five 10 µm-long straight lines per cells perpendicularly to the wound). $n = 3$ independent experiments per experimental group (15 cells per condition)

migration. Our data, differing from the data obtained in the genetic model of Sos1 ablation [18], demonstrated that BI-3406 administration did not impair the capability of primary MEFs to migrate (Fig. 8C). The potential effect of BI-3406 increasing the ability of primary MEFs to degrade gelatin was also assessed. Interestingly, pharmacologic-mediated Sos1 inhibition did not alter Mmp2 protein expression and although increased the capability of primary MEFs to degrade gelatin (Fig. 8D, E) it occurred in much less extension than that observed upon genetically-mediated Sos1 ablation.

Discussion

We have previously reported that Sos1 is required for cell migration in MEFs [18]. Accordingly, our results here presented further demonstrate that pharmacologically-mediated Sos1 inhibition impairs the capability of primary MEFs to migrate in an in vitro 2D model of wound healing. However, the mechanistic basis of Sos1 regulating this cellular process was unclear. Here, we report that Sos1 controls FA turnover and the protrusion/retraction cycle that enables cell migration as well as the ability of cells to degrade and reorganize the matrix in three-dimensional microenvironments. Sos1 depletion reduces the ability of the cell to undergo contraction, which results in deficient phosphorylation and activation of non-muscle myosin II (NMII), impaired FA maturation and loss of front-rear polarity (recently reviewed in [47, 48]).

Consistently, MEFs generated from constitutive $Sos1^{KO}$ mice [6] display similar defects to the inducible Cre model used here [26]. Moreover, other non-fibroblastic cell lines also display migratory defects upon reduction of Sos1 expression [27–29, 49, 50]. Interestingly, Sos1 depletion impairs the localization of active Rac to the leading edge, which reinforces the notion that Sos1 contributions to cell polarization Sos1 is also involved in the chemotactic response of endothelial cells to Tie-1 in a Rac-dependent manner [51].

Sos1 is a dual GEF for Ras and Rac [4, 52]. The in vivo Rac-GEF activity of Sos1 appears to be mostly mediated by its specific interaction with the E3B1 adaptor protein [7, 38]. Sos1-dependent activation of Rac requires that Sos1-E3B1 complexes are recruited to membrane ruffles to promote Rac GDP/GTP exchange locally [7, 27]. However, the mechanisms regulating Rac activation by Sos1 are still poorly understood, although they appear to be essential for the control of lamellipodial protrusion and cell migration or invasion. For example, Sos1 silencing disrupted Rac-dependent podosome assembly, subsequently impairing cell migration as observed in other cell lines such as macrophages or COS cells [27, 53]. The local nature of the regulation of Rac activation downstream of Sos1 seems local, since the levels of GTP-bound Rac were unaffected by depletion of either, or both, Sos isoforms, in response to EGF stimulation [18]. During wound healing, we postulate that Sos1 enables the activation of Rac at the leading edge while promoting cellular contraction of the cell body, enabling the haptotactic global migratory cellular response that mediates wound closure. Please note, nevertheless, that CRIB domain may interacts not only with Rac but also with other effectors such as Cdc42, RhoU or RhoV [54, 55] and then the signal detected may not fully represent, activated Rac distribution.

Traction is essential for 3D as well as 2D migration [56], hence we hypothesized that, due to their decreased contractile ability, Sos1-depleted cells would also migrate poorly in 3D. Surprisingly, Sos1-depleted cells invaded gelatin gels more easily than non-depleted cells, leading us to wonder about the mechanism that mediated such effect, which superseded the decreased contraction observed in the $Sos1^{KO}$ MEFs. One possibility was that, despite their decreased contractility, Sos1-depleted cells could reorganize the matrix more efficiently. Consistent with this, our data have revealed a previously unknown repressor activity of Sos1 on expression of Mmp2 and Mmp9 matrix metalloproteases. Both Mmps were differentially affected by depletion of Sos1, Sos2, or both Sos1 and Sos2. While simultaneous depletion of Sos1 and Sos2 increased *Mmp2* gene expression, it had no effect on *Mmp9*. Conversely, individual depletion of Sos1 and Sos2 had a modest effect on *Mmp2* expression but increased *Mmp9* levels significantly. Together with our invasion data, we postulate that $Sos1^{KO}$ cells display increased invasion due to the elevated levels of *Mmp2* and *Mmp9* despite displaying a low contractile activity; $Sos1/2^{DKO}$ cells compensate the lack of *Mmp9* induction by increasing the levels of *Mmp2*, which is the most specific Mmp for collagen of the two [57]. In addition, $Sos2^{KO}$ cells display increased invasion ability due to a combination of normal contractility combined with increased levels of both *Mmp2* and *Mmp9*. It is important to highlight that the mechanism through which Sos1/2 control the

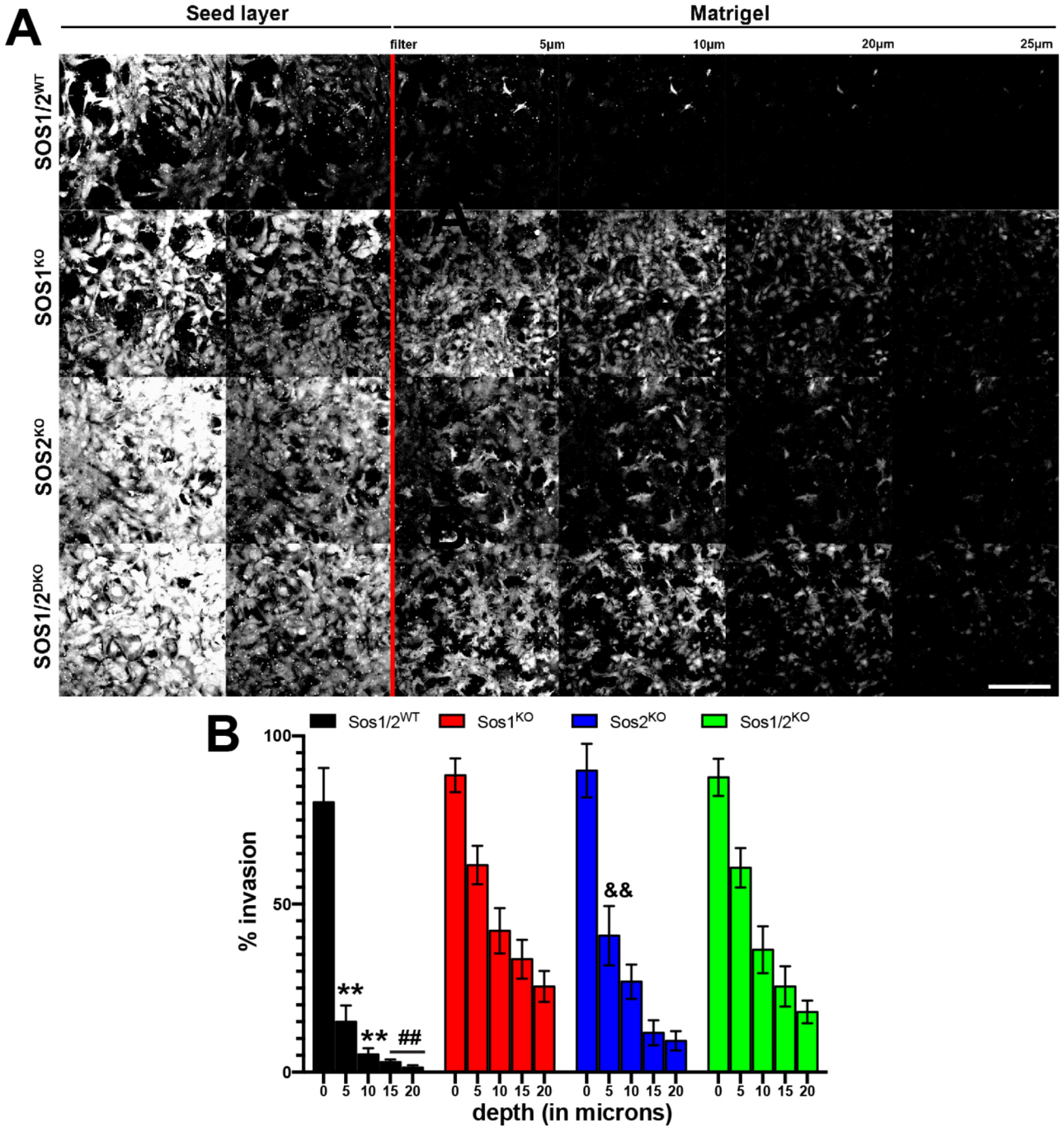

Fig. 5 Sos1/2 depletion enhances cell invasion. **(A)** Transmigration of MEFs of the indicated genotype into Matrigel plugs in an inverted invasion assay. After staining with Calcein-AM (green) living cells were visualized by confocal microscopy. Serial optical sections were acquired at 2.5 µm intervals and 5 µm intervals are shown alongside one another, with increasing depth from left to right as indicated. Scale bar: 100 µm. **(B)** Quantification of invasion is expressed as percentage of the field covered with cells at the indicated depths. Data shown are means ± SD of two independent experiments. One-way ANOVA and Tukey's multiple comparison test was applied. $^{**}p < 0.01$ vs. the rest of experimental groups; ## $p < 0.01$ vs. $Sos1^{KO}$ and $Sos1/2^{DKO}$

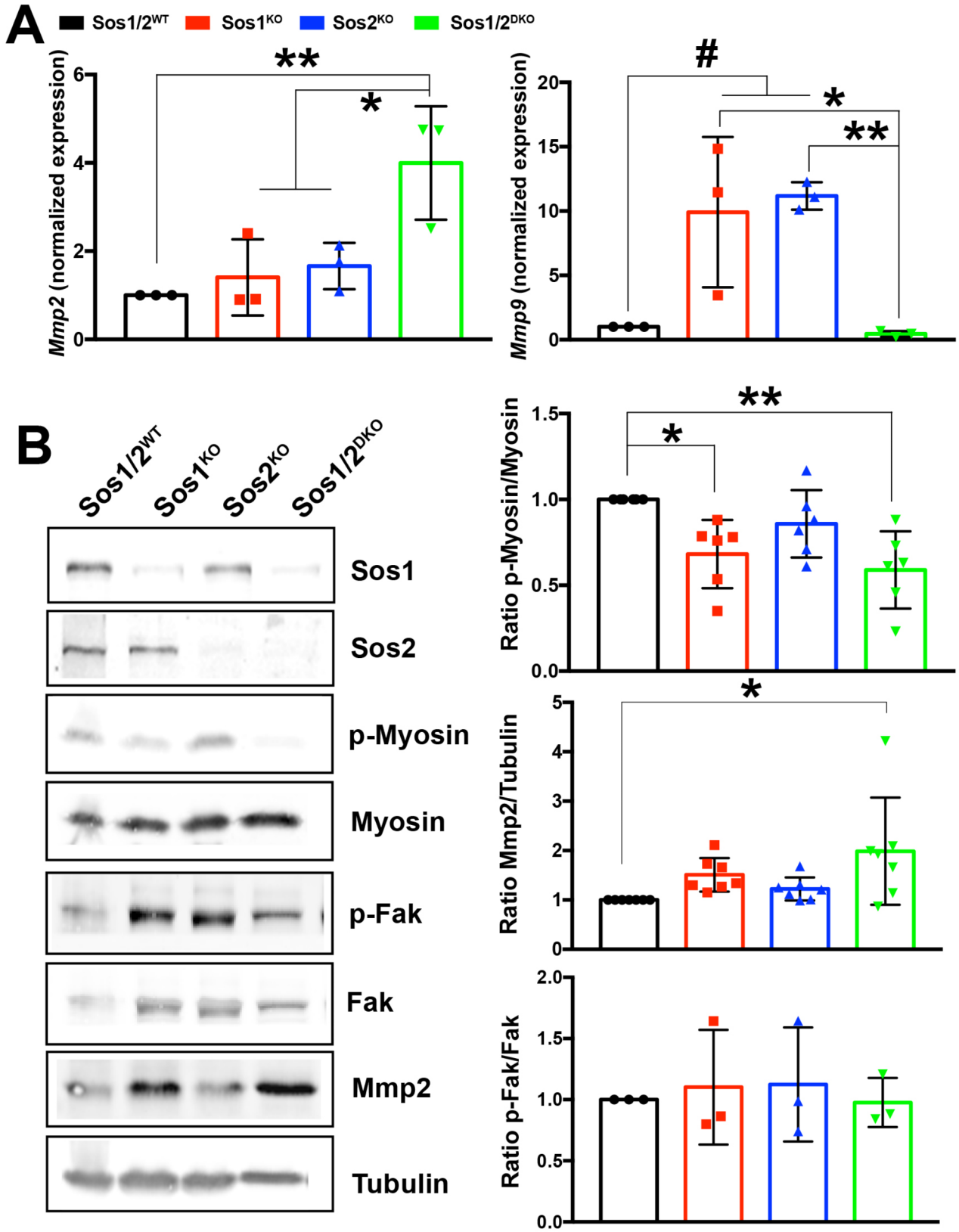

Fig. 6 (See legend on next page.)

(See figure on previous page.)

Fig. 6 Sos1/2- depletion increased Mmp2/9 expression. **(A)**. Quantification of mRNA expression levels of *Mmp2 and Mmp9* in primary MEFs of the indicated Sos genotypes by RT-qPCR. *β-actin* was used as internal control for normalization. $n=3$ independent samples per genotype. Data expressed as mean ± SD. *$p<0.05$ and **$p<0.01$ vs. Sos1/2^{DKO}; #$p<0.05$ vs. Sos1/2^{WT}. **(B)** Representative western blots of Sos1, Sos2, phospho-Myosin, phospho-Fak, total Myosin, total Fak, and Mmp2 protein expression, using Tubulin as a control for normalization. Bar charts illustrate the quantitation of the ratio of phospho-myosin levels relative to total myosin and the ratio of Mmp2 protein expression relative to Tubulin expression in MEFs of all Sos1/2 genotypes. $n=3$ per genotype. Data shown as mean ± SD. *$p<0.05$ and **$p<0.01$ vs. Sos1/2^{DKO}. && $p<0.01$ vs. Sos1^{KO} and Sos1/2^{DKO}

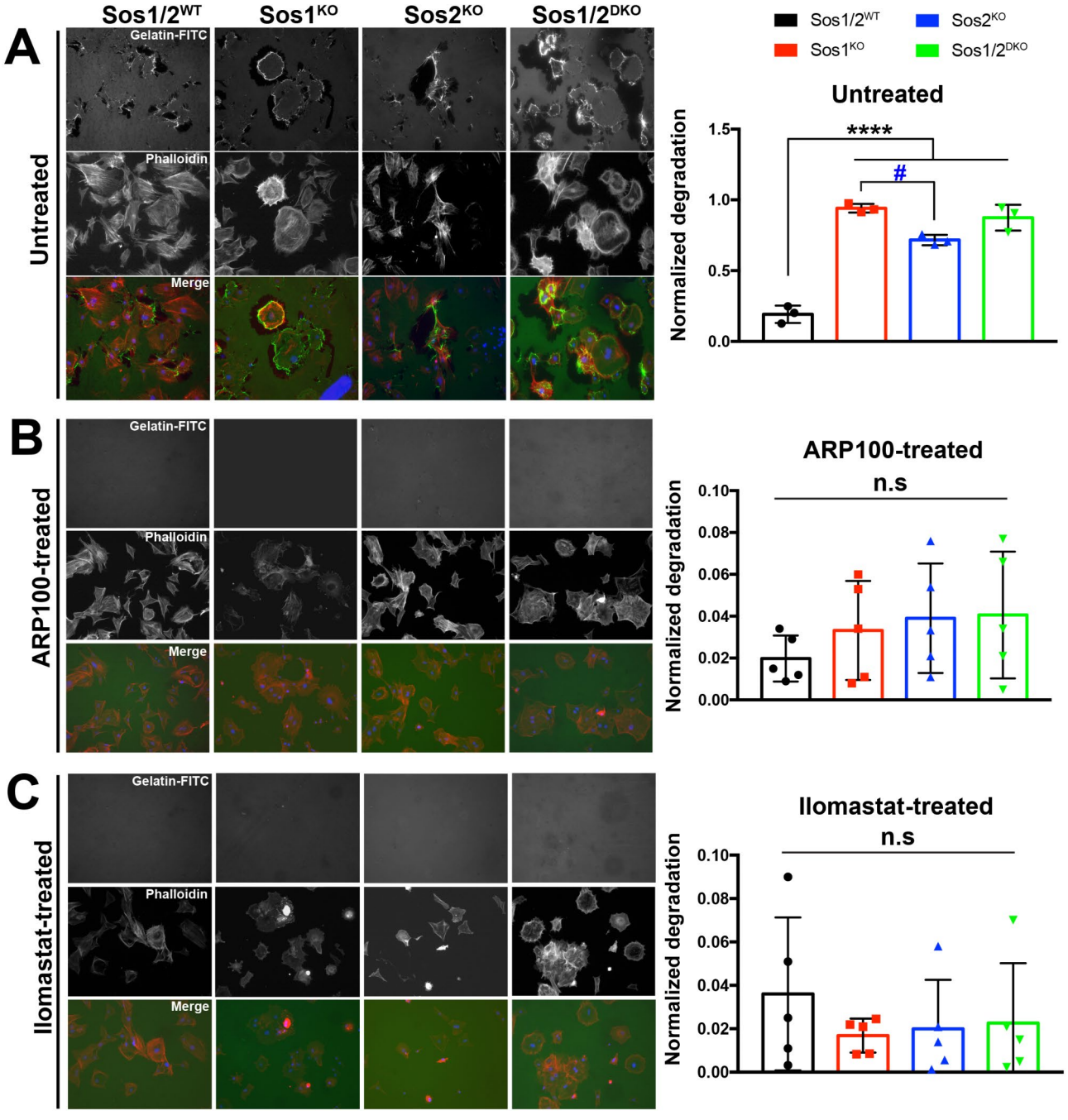

Fig. 7 Mmp2/9 inhibitors block Sos1/2-dependent gelatin degradation. **(A)** 12 days 4OHT-treated MEFs of the four defined genotypes were seeded on gelatin-FITC-coated coverslips for 8 h and then fixed. The graph illustrates the mean area of gelatin degradation (black areas). Data shown as mean ± SD. $n=3$ independent experiments per genotype (a total of 50 cells were quantitated per experiment). ****$p<0.0001$ vs. Sos1/2^{WT}, #$p<0.05$ vs. Sos1^{KO}. **(B-C)** Primary MEFs treated as in A were plated on gelatin-FITC-coated coverslips and pre-treated with ARP100 (**B**) or Ilomastat (**C**) as indicated in the Material and Methods section, 3 h after seeding. The cells were then fixed after 16 h. The graph illustrates the mean area of gelatin degradation (black areas). Data shown as mean ± SD. n.s: not significant. $n=5$ independent experiments per genotype (a total of 50 cells were quantitated per experiment)

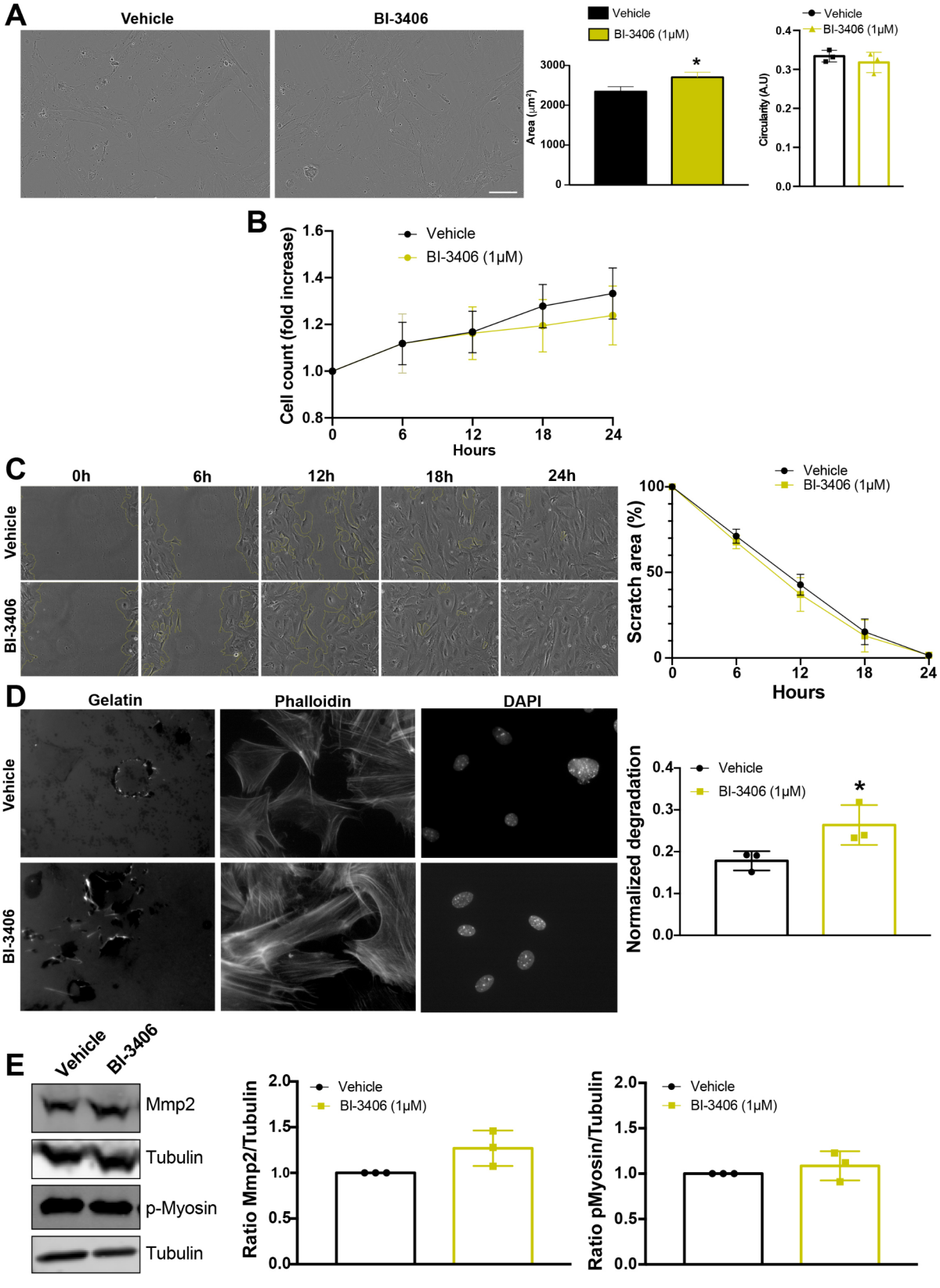

Fig. 8 (See legend on next page.)

(See figure on previous page.)

Fig. 8 The Sos1 inhibitor BI-3406 does not mimic the effects of genetically-mediated Sos1 depletion. **(A)** Representative images of DMSO or BI-3406-treated WT primary MEFs for 24 h taken from Incucyte. The graphs show the mean cell area as well as the circularity of MEFs in both experimental groups. Circularity ranges from 0 to 1, being 1 a perfect circumference. Data shown as mean ± SD. $n = 3$ independent experiments per condition (50 cells/group). * $p < 0.05$ vs. vehicle-treated group. Scale Bar: 100 µm. **(B)** Growth curve of vehicle- or BI-3406-treated (24 h) primary MEFs in culture measured with Incucyte. Data shown as mean ± SD. $n = 3$ independent experiments per condition. **(C)** Vehicle- (DMSO) or BI-3406-treated (1µM) confluent WT primary MEFs were scratched with a micropipette tip and closure of the wounded area was recorded for 24 h by phase-contrast photomicroscopy (×10 magnification). Areas where cellular growth is not yet recovered after the wound are marked by surrounding yellow lines. Data shown as mean ± SD. $n = 3$ independent experiments per condition. * $p < 0.05$ vs. vehicle-treated group. **(D)** Vehicle- (DMSO) or BI-3406-treated (1µM) MEFs of the WT genotype were seeded on gelatin-FITC-coated coverslips for 8 h, fixed and then counterstained with phalloidin and DAPI. The bar chart illustrates the mean area of gelatin degradation (black areas). Data shown as mean ± SD. $n = 3$ independent experiments per condition (a total of 30 cells were quantitated per experiment). * $p < 0.05$ vs. vehicle-treated counterpart. **(E)** Western blots from protein extracts of Vehicle- or BI-3406-administered (24 h) MEFs, of Mmp2 and phospho-Myosin protein expression, using Tubulin as a control for normalization,. Bar charts illustrate the quantitation of the ratio of Mmp2 and phospho-Myosin levels relative to Tubulin. Data shown as mean ± SD. $n = 3$ independent experiments per condition

expression of Mmp2/9 is currently unknown and will require further analysis.

Finally, given the importance of the recently reported Sos1 inhibitors as potential therapeutic tools in certain RAS-driven malignancies [4, 25], we further evaluated the effect of the Sos1 inhibitor BI-3406 in different cellular processes in primary MEFs. Our results demonstrated that, in contrast to the results obtained following genetically-mediated Sos1 ablation [18], BI-3406 barely altered the cell architecture of primary MEFs and did not impair cell proliferation or cell migration in this cell type. BI-3406 administration increased the capacity of primary MEFs to degrade gelatin, but much less in comparison with the genetic model of Sos1 removal. Overall, these observations suggest that BI-3406 does not recapitulate the effects observed when Sos1 is genetically ablated. In this regard, prior studies revealed that BI-3406 preferably blocks interaction of Sos1 with oncogenic Ras alleles (mainly KRas), whereas it shows no antiproliferative properties in Ras WT tumor cells [24], suggesting that this compound preferably acts over oncogenic, KRas-dependent, tumor cells. In addition, whereas BI-3406 has been proven to bind to the catalytic domain of SOS1, thereby preventing the interaction with KRas, it has not been evaluated whether it may interfere Sos1-mediated Rac activation. Our wound-healing assays suggest the BI-3406 probably does not disrupt Sos1-Rac interaction. Nevertheless, further experiments are needed, particularly in Kras-mutant cells, in order to evaluate whether these small molecules could impact the capability of tumor cells to migrate.

Conclusions

Our present results add new, detailed information regarding the functional contribution of Sos1/2, and especially of Sos1, to the regulation of cell migration, which seem to differ if analyzed under 2D or 3D conditions. In this regard, our data also unveiled a possible involvement of Sos1/2 in the regulation of Mmp2/9 in primary MEFs.

Abbreviations

CRIB	Cdc42- and Rac-Interactive Binding motif
DEG	Differentially Expressed Genes
DKO	Double Knock-Out
ECM	ExtraCellular Matrix
FAs	Focal Adhesions
GDP	Guanosine Diphosphate
GEF	Guanine nucleotide Exchange Factor
GTP	Guanosine Triphosphate
IRM	Interference Reflection Microscopy
KO	Knock-Out
MEFs	Mouse Embryonic Fibroblasts
MMP	Matrix MetalloProteinase
PBS	Phosphate Buffered Saline
SOS	Son Of Sevenless
4OHT	4-HydroxyTamoxifen
WT	Wild Type

Supplementary Information

The online version contains supplementary material available at https://doi.org/10.1186/s12964-025-02122-1.

Supplementary Material 1

Author contributions

Conception and Design: F.C.B, E.S, P.L.B, M.V-M and A.J.R. Data acquisition, analysis, and validation: P.L.B, R.G.-N, C. LI, L.F.L.-M, R.F.-M, N.C, F.M.V, L.L-R, M.R.H, A.J.R, M.V.-M, F.C.B. Drafting manuscript: E.S, F.C.B. Revising manuscript: E.S, F.C.B, P.L.B, R.G-N, L.F.L.-M, R.F.-M, F.M.V, A.J.R, X.R.B, M.V-M.

Funding

This work was funded by grants ISCIII-MCUI (FIS PI19/00934), JCyL (SA264P18-UIC 076), Areces Foundation (CIVP19A5942) and ISCIII-CIBERONC (group CB16/12/00352) to E.S; Solórzano-Barruso Foundation (FS/32-2020), Ministerio de Ciencia e Innovación (MICIU/AEI/https://doi.org/10.13039/501100011033/, as part of I + D + i Project "PID2022-136409OB-I00" and MICIU/AEI/https://doi.org/10.13039/501100011033/ and NextGenerationEU/PRTR, as part of I + D + i Project "CNS2022-135292), Eugenio Rodriguez Pascual Foundation and Asociación Inés de Pablo Llorens-GETTHI to F.C.B; Federación Española de Enfermedades Raras (AI-2023-015) to F.M.V; Ministerio de Ciencia e Innovación (PID2020-116232RB-I00) and ECRIN-M3 from AECC/AIRC/CRUK to M.V-M; Cancer Research UK (C6620/A15961) to A.J.R. The X.R.B.'s project leading to these results has received funding from the AECC (GC16173472GARC), the Castilla-León government (CSI018P23), grants funded by MCIN/AEI/https://doi.org/10.13039/501100011033/ plus the European Research Development Fund «A way of making Europe» of the European Union (PID2021-122666OB-I00, PDC2022-133027-I00, PLEC2022-009217), «la Caixa» Banking Foundation (HR20-00164), and the «Escalera de Excelencia» of the Education Ministry of the Castilla y León autonomous government plus the European Research Development Fund (CLU-2023-2-01). This research was co-financed by FEDER funds. These CIC groups are supported by the Programa de Apoyo a Planes Estratégicos de Investigación de Estructuras de Investigación de Excelencia of Castilla y León autonomous government (CLC-2017-01) and AECC Excellence program Stop RAS Cancers (EPAEC222641CICS).

Data availability
All microarray raw data have been uploaded and are accessible at the NCBI Gene Expression Omnibus (GEO) database (GSE277505).

Declarations

Ethical approval and consent to participate
All experiments were approved by the Bioethics Committee of the Cancer Research Center (#417).

Competing interests
The authors declare no competing interests.

Author details
[1]Lab 1, Centro de Investigación del Cáncer - IBMCC (CSIC-USAL) and CIBERONC, Universidad de Salamanca, Salamanca 37007, Spain
[2]Molecular Mechanisms Program, Centro de Investigación del Cáncer, Instituto de Biología Molecular y Celular del Cáncer, Consejo Superior de Investigaciones Científicas (CSIC) and University of Salamanca, Salamanca 37007, Spain
[3]Ecole Polytechnique fédérale de Lausanne, Lausanne, Switzerland
[4]Departamento de Fisiología Medica y Biofísica, Facultad de Medicina, Universidad de Sevilla and Instituto de Biomedicina de Sevilla (IBiS) (Hospital Universitario Virgen del Rocío, CSIC/Universidad de Sevilla), Sevilla 41013, Spain
[5]Departamento de Biología Celular, Facultad de Biología, Universidad de Sevilla and Instituto de Biomedicina de Sevilla (IBiS) (Hospital Universitario Virgen del Rocío, CSIC/Universidad de Sevilla), Sevilla 41012, Spain
[6]Randall Centre of Cell and Molecular Biophysics, King's College London, Guy's Campus, New Hunt's House, London SE1 1UL, UK
[7]School of Cellular and Molecular Medicine, Biomedical Sciences Building, University Walk, University of Bristol, Bristol BS8 1TD, UK
[8]Lab 2, Centro de Investigación del Cáncer - IBMCC (CSIC-USAL) and CIBERONC, Universidad de Salamanca, Salamanca 37007, Spain

Received: 24 October 2024 / Accepted: 23 February 2025
Published online: 03 March 2025

References

1. Buday L, Downward J. Many faces of Ras activation. Biochim Biophys Acta. 2008;1786:178–87.
2. Castellano E, Santos E. Functional specificity of Ras isoforms: so similar but so different. Genes Cancer. 2011;2:216–31.
3. Cherfils J, Zeghouf M. Regulation of small GTPases by GEFs, gaps, and GDIs. Physiol Rev. 2013;93:269–309.
4. Baltanás FC, Zarich N, Rojas-Cabañeros JM, Santos E. SOS GEFs in health and disease. Biochim. Biophys. Acta - Rev Cancer. 2020.
5. Baltanás FC, García-Navas R, Santos E. Sos2 comes to the fore: differential functionalities in physiology and pathology. Int J Mol Sci. 2021.
6. Qian X, Esteban L, Vass WC, Upadhyaya C, Papageorge AG, Yienger K, et al. The Sos1 and Sos2 Ras-specific exchange factors: differences in placental expression and signaling properties. Embo J. 2000;19:642–54.
7. Innocenti M, Tenca P, Frittoli E, Faretta M, Tocchetti A, Di Fiore PP, et al. Mechanisms through which Sos-1 coordinates the activation of Ras and Rac. J Cell Biol. 2002;156:125–36.
8. Gerboth S, Frittoli E, Palamidessi A, Baltanas FC, Salek M, Rappsilber J, et al. Phosphorylation of SOS1 on tyrosine 1196 promotes its RAC GEF activity and contributes to BCR-ABL leukemogenesis. Leukemia. 2018;32:820–7.
9. Kortum RL, Sommers CL, Alexander CP, Pinski JM, Li W, Grinberg A, et al. Targeted Sos1 deletion reveals its critical role in early T-cell development. Proc Natl Acad Sci U S A. 2011;108:12407–12.
10. Baltanás FC, Pérez-Andrés M, Ginel-Picardo A, Diaz D, Jimeno D, Liceras-Boillos P, et al. Functional redundancy of Sos1 and Sos2 for lymphopoiesis and organismal homeostasis and survival. Mol Cell Biol. 2013;33:4562–78.
11. Theard PL, Linke AJ, Sealover NE, Daley BR, Yang J, Cox K, et al. SOS2 modulates the threshold of EGFR signaling to regulate osimertinib efficacy and resistance in lung adenocarcinoma. Mol Oncol. 2024;18:641–61.
12. García-Navas R, Liceras-Boillos P, Gómez C, Baltanás FC, Calzada N, Nuevo-Tapioles C, et al. Critical requirement of SOS1 RAS-GEF function for mitochondrial dynamics, metabolism, and redox homeostasis. Oncogene. 2021;40:4538–51.
13. Gómez C, Garcia-Navas R, Baltanás FC, Fuentes-Mateos R, Fernández-Medarde A, Calzada N, et al. Critical requirement of SOS1 for development of BCR/ABL-Driven chronic myelogenous leukemia. Cancers (Basel). 2022;14:3893.
14. Baltanas FC, Kramer-Drauberg M, Garcia-Navas R, Patrucco E, Petrini E, Arnhof H et al. Pharmacological SOS1 inhibitor BI-3406 demonstrates in vivo anti-tumor activity comparable to SOS1 genetic ablation in KRAS mutant tumors. bioRxiv [Internet]. 2024;2024.09.18.613686. Available from: http://biorxiv.org/content/early/2024/09/22/2024.09.18.613686.abstract.
15. Daley BR, Sealover NE, Finniff BA, Hughes JM, Sheffels E, Gerlach D et al. SOS1 Inhibition enhances the efficacy of KRASG12C inhibitors and delays resistance in lung adenocarcinoma. Cancer Res. 2024.
16. Daley BR, Vieira HM, Rao C, Hughes JM, Beckley ZM, Huisman DH et al. SOS1 and KSR1 modulate MEK inhibitor responsiveness to target resistant cell populations based on PI3K and KRAS mutation status. Proc Natl Acad Sci U S A. 2023;120.
17. Sheffels E, Sealover NE, Theard PL, Kortum RL. Anchorage-independent growth conditions reveal a differential SOS2 dependence for transformation and survival in RAS-mutant cancer cells. Small GTPases. 2021;12:67–78.
18. Liceras-Boillos P, García-Navas R, Ginel-Picardo A, Anta B, Pérez-Andrés M, Lillo C et al. Sos1 disruption impairs cellular proliferation and viability through an increase in mitochondrial oxidative stress in primary MEFs. Oncogene 2016;1–14.
19. Liceras-Boillos P, Jimeno D, García-Navas R, Lorenzo-Martín LF, Menacho-Marquez M, Segrelles C, et al. Differential role of the RasGEFs Sos1 and Sos2 in mouse skin homeostasis and carcinogenesis. Mol Cell Biol. 2018;38:e00049–18.
20. Suire S, Baltanas FC, Segonds-Pichon A, Davidson K, Santos E, Hawkins PT, et al. Frontline science: TNF-α and GM-CSF1 priming augments the role of SOS1/2 in driving activation of Ras, PI3K-γ, and neutrophil Proinflammatory responses. J Leukoc Biol. 2019;106:815–22.
21. Baltanás FC, Mucientes-Valdivieso C, Lorenzo-Martín LF, Fernández-Parejo N, García-Navas R, Segrelles C, et al. Functional specificity of the members of the Sos family of Ras-GEF activators: novel role of Sos2 in control of epidermal stem cell homeostasis. Cancers (Basel). 2021;13:2152.
22. Baltanás FC, García-Navas R, Rodríguez-Ramos P, Calzada N, Cuesta C, Borrajo J, et al. Critical requirement of SOS1 for tumor development and microenvironment modulation in KRASG12D-driven lung adenocarcinoma. Nat Commun. 2023;14:5856.
23. Hillig RC, Bader B. Targeting RAS oncogenesis with SOS1 inhibitors. Adv Cancer Res. 2022. pp. 169–203.
24. Hofmann MH, Gmachl M, Ramharter J, Savarese F, Gerlach D, Marszalek JR, et al. BI-3406, a potent and selective SOS1::KRAS interaction inhibitor, is effective in KRAS-driven cancers through combined MEK Inhibition. Cancer Discov. 2021;11:142–57.
25. Hofmann MH, Gerlach D, Misale S, Petronczki M, Kraut N. Expanding the reach of precision oncology by drugging all KRAS mutants. Cancer Discov. 2022;12:924–37.
26. Fuentes-Calvo I, Martinez-Salgado C. Sos1 modulates extracellular matrix synthesis, proliferation, and migration in fibroblasts. Front Physiol. 2021;12.
27. Baruzzi A, Remelli S, Lorenzetto E, Sega M, Chignola R, Berton G. Sos1 regulates macrophage podosome assembly and macrophage invasive capacity. J Immunol. 2015;195:4900–12.
28. Goicoechea S, Arneman D, Disanza A, Garcia-Mata R, Scita G, Otey CA. Palladin binds to Eps8 and enhances the formulation of dorsal ruffles and podosomes in vascular smooth muscle cells. J Cell Sci. 2006;119:3316–24.
29. Guittard G, Kortum RL, Balagopalan L, Çuburu N, Nguyen P, Sommers CL, et al. Absence of both Sos-1 and Sos-2 in peripheral CD4 +T cells leads to PI3K pathway activation and defects in migration. Eur J Immunol. 2015;45:2389–95.
30. Esteban LM, Fernández-Medarde A, López E, Yienger K, Guerrero C, Ward JM, et al. Ras-guanine nucleotide exchange factor sos2 is dispensable for mouse growth and development. Mol Cell Biol. 2000;20:6410–3.
31. Holt MR, Calle Y, Sutton DH, Critchley DR, Jones GE, Dunn GA. Quantifying cell-matrix adhesion dynamics in living cells using interference reflection microscopy. J Microsc. 2008;232:73–81.
32. Barr VA, Bunnell SC. Interference reflection microscopy. Curr Protoc Cell Biol. 2009.

33. Díaz B. Invadopodia detection and gelatin degradation assay. BIO-PROTOCOL. 2013;3.
34. Scott RW, Crighton D, Olson MF. Modeling and imaging 3-dimensional collective cell invasion. J Vis Exp. 2011.
35. García E, Machesky LM, Jones GE, Antón IM. WIP is necessary for matrix invasion by breast cancer cells. Eur J Cell Biol. 2014;93:413–23.
36. Parsons JT, Horwitz AR, Schwartz MA. Cell adhesion: integrating cytoskeletal dynamics and cellular tension. Nat Rev Mol Cell Biol. 2010. pp. 633–43.
37. Ridley AJ, Schwartz MA, Burridge K, Firtel RA, Ginsberg MH, Borisy G et al. Cell migration: integrating signals from front to back. Science. 2003. pp. 1704–9.
38. Scita G, Nordstrom J, Carbone R, Tenca P, Giardina G, Gutkind S, et al. EPS8 and E3B1 transduce signals from Ras to Rac. Nature. 1999;401:290–3.
39. Miroshnikova YA, Mouw JK, Barnes JM, Pickup MW, Lakins JN, Kim Y, et al. Tissue mechanics promote IDH1-dependent HIF1α-tenascin C feedback to regulate glioblastoma aggression. Nat Cell Biol. 2016;18:1336–45.
40. Aguilar-Cuenca R, Llorente-González C, Chapman JR, Talayero VC, Garrido-Casado M, Delgado-Arévalo C, et al. Tyrosine phosphorylation of the myosin regulatory light chain controls Non-muscle myosin II assembly and function in migrating cells. Curr Biol. 2020;30:2446–e24586.
41. Friedl P, Wolf K. Plasticity of cell migration: A multiscale tuning model. J Cell Biol. 2010. pp. 11–9.
42. Lauffenburger DA, Horwitz AF. Cell migration: A physically integrated molecular process. Cell. 1996. pp. 359–69.
43. Chen P, Parks WC. Role of matrix metalloproteinases in epithelial migration. J Cell Biochem. 2009. pp. 1233–43.
44. Zhang L, Shi J, Feng J, Klocker H, Lee C, Zhang J. Type IV collagenase (matrix metalloproteinase-2 and– 9) in prostate cancer. Prostate Cancer Prostatic Dis. 2004;7:327–32.
45. Bonnans C, Chou J, Werb Z. Remodelling the extracellular matrix in development and disease. Nat Rev Mol Cell Biol. 2014. pp. 786–801.
46. Paralkar VM, Vukicevic S, Reddi AH. Transforming growth factor B type 1 binds to collagen IV of basement membrane matrix: implications for development. Dev Biol. 1991;143:303–8.
47. Garrido-Casado M, Asensio-Juárez G, Talayero VC, Vicente-Manzanares M. Engines of change: nonmuscle myosin II in mechanobiology. Curr Opin Cell Biol. 2024.
48. Garrido-Casado M, Asensio-Juárez G, Vicente-Manzanares M. Nonmuscle myosin II regulation directs its multiple roles in cell migration and division. Annu Rev Cell Dev Biol. 2021. pp. 285–310.
49. Cheng M, Ye X, Dai J, Sun F. SOS1 promotes epithelial-mesenchymal transition of epithelial ovarian Cancer (EOC) cells through AKT independent NF-κB signaling pathway. Transl Oncol. 2021;14.
50. Li Y, Yin Y, He Y, He K, Li J. SOS1 regulates HCC cell epithelial-mesenchymal transition via the PI3K/AKT/mTOR pathway. Biochem Biophys Res Commun. 2022;637.
51. Cascone I, Audero E, Giraudo E, Napione L, Maniero F, Philips MR, et al. Tie-2-dependent activation of RhoA and Rac1 participates in endothelial cell motility triggered by angiopoietin-1. Blood. 2003;102:2482–90.
52. Nimnual A, Bar-Sagi D. The two hats of SOS. Sci STKE. 2002.
53. Hwang HS, Hwang SG, Cho JH, Chae JS, Yoon KW, Cho SG, et al. CIIA functions as a molecular switch for the Rac1-specific GEF activity of SOS1. J Cell Biol. 2011;195:377–86.
54. Burbelo PD, Drechsel D, Hall A. A conserved binding motif defines numerous candidate target proteins for both Cdc42 and Rac GTPases. J Biol Chem J Biol Chem. 1995;270:29071–4.
55. Hodge RG, Ridley AJ. Regulation and functions of RhoU and RhoV. Small GTPases. Taylor and Francis Inc.; 2020. pp. 8–15.
56. Thomas DG, Yenepalli A, Denais CM, Rape A, Beach JR, Wang Y, Ii, et al. Non-muscle myosin IIB is critical for nuclear translocation during 3D invasion. J Cell Biol. 2015;210:583–94.
57. Hey S, Linder S. Matrix metalloproteinases at a glance. J Cell Sci Co Biologists Ltd; 2024;137.

Publisher's note